A new one-pot hydrothermal synthesis and electrochemical characterization of $Li_{1+x}Mn_{2-y}O_4$ spinel structured compounds†

Brendan J. Liddle, Sean M. Collins and Bart M. Bartlett*

A simple one step hydrothermal route to $Li_{1+x}Mn_{2-y}O_4$ spinel compounds ($x = 0.01$–0.06, $y = 0.02$–0.09) *via* reduction of commercially available potassium permanganate with common organic reductants (alcohols, acetone, hex-1-ene, and isobutyraldehyde) in lithium hydroxide aqueous solutions is developed. The cubic spinel phase with no other impurities can be isolated after short reaction times (~5 h) at the relatively low temperature of 180 °C. Scanning electron microscopy imaging reveals that the crystalline products have a distribution of sizes; the majority of the sample is composed of smaller particles between 10 and 30 nm. However, there are noticeably larger 100–300 nm interspersed particles—more prevalent in reactions with acetone and isobutyraldehyde. In corresponding benchtop test reactions, UV-Vis spectroscopy shows that the disappearance of MnO_4^- occurs more rapidly when acetone and isobutyraldehyde are used as reducing agents. Cyclic voltammetry performed on our spinels prepared *via* hydrothermal synthesis shows three reversible redox processes: a wave with $E_{1/2}$ of ~2.9 V (*vs.* Li/Li⁺) and two close waves between 4.05 and 4.15 V. Galvanostatic cycling of a cell composed of $Li_{1.02}Mn_{1.96}O_4$ prepared from the oxidation of acetone between 3.5 and 4.4 V demonstrates a specific capacity of 104 mA h g⁻¹ on first discharge, with ~87% capacity retention (90 mA h g⁻¹) after 100 cycles. The specific capacity of all samples correlates with the rate of disappearance of MnO_4^- observed in our benchtop reactions, providing a facile way to control particle size and electrochemical behavior.

Introduction

Lithium ion secondary cells have garnered a great deal of research focus due mainly to higher possible energy densities than NiMH and lead acid technologies.[1–3] Because of their low cost, low toxicity, and low internal resistance, lithium manganese oxide $LiMn_2O_4$ with the spinel structure has become a very attractive material for use as lithium insertion cathodes.[4–7] $LiMn_2O_4$ has a high specific (or gravimetric) energy density of

University of Michigan, Department of Chemistry, 930 N. University Avenue, Ann Arbor, MI, 48109-1055, USA. E-mail: bartmb@umich.edu; Fax: +1 (734) 647 4865; Tel: +1 (734) 615 9279

† Electronic supplementary information (ESI) available: X-Ray diffraction data including Rietveld refinement of the XRD patterns, cyclic voltammetry and chronopotentiometry, elemental analyses, and redox titration data for all compounds presented in this study. See DOI: 10.1039/c0ee00059k

293 mA h g⁻¹. Lithium can be electrochemically extracted at ~4.1 V to yield $Li_{1-x}Mn_2O_4$, or inserted at 2.9 V giving $Li_{1+x}Mn_2O_4$. However, severe capacity fade occurs during galvanostatic cycling between 3.6 and 2.9 V, attributed to two phenomena: (1) a cubic to tetragonal phase change understood by Jahn–Teller distortion of Mn^{3+} ions at the end of discharge and (2) solubility of spinel by acid attack from the electrolyte, resulting in disproportionation of Mn^{3+} at the crystallite surface. Mn^{2+} is highly soluble in the polycarbonate electrolyte solutions used in the cell.[8,9] This limits the practical use of the material to lithium extraction at 4 V. Therefore, the maximum available capacity is only 148 mA h g⁻¹, still comparable to the observed capacity of the widely used $LiCoO_2$ (120–150 mA h g⁻¹).[10,11]

Although the compound $LiMn_2O_4$ was originally prepared over 60 years ago from high temperature calcination of Li_2CO_3 and $MnCO_3$, many different methods have since been reported for its synthesis.[12–15] However, recent emphasis has been placed

---

Broader context

The oil crisis of 1970s brought to the forefront the need to develop alternative sources of energy. As fossil fuel reserves are depleted with environmental pollutants and climate change associated with their combustion, a great deal of emphasis has been placed on developing carbon neutral, renewable energy processes such as solar and wind energy conversion technologies. One roadblock to the widespread use of these energy conversion technologies is the lack of efficient and cost-effective methods for storing this energy. Batteries play an important role as energy storage devices because they can directly deliver stored energy as d.c. electricity to portable devices such as cellular phones and automobiles. Spinel structures based on manganese have attracted attention as cathode materials for many years because they undergo two redox processes. However, irreversible phase changes prevent both redox processes from doing useful electrical work. New synthetic methods allow for simultaneous control of particle size and chemical composition to recover some of this capacity.
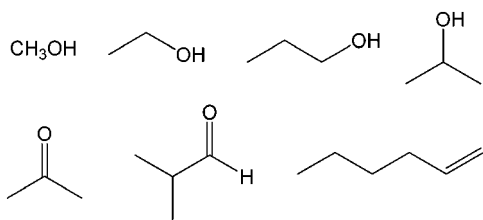
Fig. 1 Organic reducing agents employed in this study.

on methods that give nanosized or nanostructured materials due to their greater cyclability as a result of a shorter Li^+ diffusion length. Moreover, smaller particles better accommodate unit cell volume changes upon battery cycling. For example, a recently reported synthesis of $LiMn_2O_4$ nanoparticles gave a material with an observed capacity of 111 mA h g^{-1} and high rate capability. However, this synthesis involves preparing a precursor compound followed by a seven day hydrothermal treatment.[16] Because particle size and morphology are factors that depend on the nature of the synthesis, there is still a need for methods that do not require costly reagents, high temperatures, or multi-step procedures while still giving high quality nanoscale particles.

Permanganate compounds have attracted research interest as synthons for the hydrothermal synthesis of a variety of manganese oxides.[17–19] Hydrothermal decomposition of lithium permanganate has been shown to give layered and tunnel structure of manganese oxides depending on factors such as pH, reagent concentrations, and cation.[20–22] However, $LiMnO_4$ is dangerous to store and to work with; it is not thermally stable, violently decomposing to give MnO_2 and Li_2O.[23] Other reported permanganate reactions require preliminary steps—a separate reduction of permanganate or ion exchange starting from water insoluble precursors such as cetyltrimethylammonium—prior to hydrothermal treatment with LiOH.[24] Since permanganate must be reduced at relatively low temperatures for hydrothermal reactions, we explored a series of simple, unsaturated or functionalized organic compounds as mild permanganate reductants (Fig. 1). Herein, we demonstrate that nanocrystalline $LiMn_2O_4$ can be synthesized hydrothermally from a one-pot reaction in just five hours using the safe, convenient and abundant precursor, potassium permanganate, along with a variety of organic reductants. Advantages of this synthetic approach are three-fold: (1) reduction of permanganate does not need to occur in a separate reaction; (2) potassium permanganate in the synthesis does not interfere with spinel formation or lead to the formation of impurity phases; and (3) all of our starting materials are soluble in water, thus particle size is not limited by the mechanical grinding of solid MnO_2.

Experimental

General considerations

Potassium permanganate 99.0% was purchased from J. T. Baker. Lithium hydroxide 98%, lithium hexafluorophosphate, ethylene carbonate and diethyl carbonate were purchased from Aldrich. Lithium foil was obtained from Strem. All starting materials were used as received. Powder X-ray diffraction patterns were obtained with a Brüker D8 Advance diffractometer equipped

with a Lynx-Eye detector and parallel beam optics using Cu-Kα radiation ($\lambda = 1.54184$ Å). XRD patterns were indexed and refined using the TOPAS program from Brüker AXS. Scanning electron microscopy images were obtained using a FEI Nova Nanolab SEM/FIB with an accelerating voltage of 10 kV. Manganese oxidation states were determined by redox titration in which 20 mg samples were digested in 0.020 M $FeCl_2$ solutions of 10% H_2SO_4 that were titrated potentiometrically against 4.68 mM $KMnO_4$. UV-Vis spectra were recorded in 1 cm quartz cuvettes using a Varian-Cary 5000 spectrophotometer. ^{1}H-NMR spectra were recorded on a Varian 500 MHz spectrometer.

Synthesis

The spinel structured compounds in this study were prepared by hydrothermal treatment of 0.158 g (1.00 mmol) $KMnO_4$ in 13 mL 0.1 M $LiOH_{(aq)}$ along with 1.1 equivalents of the desired organic reducing agent. Reactions were carried out in 23 mL PTFE lined, stainless-steel autoclaves that were heated at a rate of 10 °C min^{-1} to a dwell temperature of 180 °C. After five hours, reactions were cooled to room temperature at a rate of 1 °C min^{-1}. The resulting dark green microcrystalline powders were collected by vacuum filtration through 0.2 μm Millipore™ filters. The precipitates were washed several times with deionized water before being dried overnight in a vacuum oven at 130 °C. Isolated yields were 90–95% based on starting permanganate.

Elemental analysis

ICP-AES elemental analysis for Li and Mn was obtained using a Perkin-Elmer Optima 2000DV. 20 mg samples were digested in 3–5 mL conc. HNO_3 with a few drops of 30% H_2O_2. Samples were referenced to an yttrium internal standard and concentrations of Li and Mn were determined from maximum line intensities compared to those of reference solutions. Li was measured at 610.632 nm; Mn was measured at 257.610 nm.

Electrochemical measurements

Active cathode mixtures were prepared by mixing the cathode material with carbon black with an agate mortar and pestle followed by adding and further mixing with polytetrafluoroethylene (PTFE) beads to give a 70 : 25 : 5 ratio by mass mixture. This material was pressed onto a stainless steel disc used in a Swagelok™ cell. Lithium foil was used as the anode, separated from the cathode by a layer of Celgard™ poly(propylene) film and Whatman No. 40 filter paper. The electrolyte solution was 1 M $LiPF_6$ in 1 : 1 ethylene carbonate and diethyl carbonate. Cell assembly was carried out under argon atmosphere in a dry-box. Cyclic voltammetry measurements were performed on a CH Instruments 660C electrochemical workstation at a scan rate of 0.1 mV s^{-1}. Gvalanostatic charge/discharge curves were recorded on a custom-designed Vencon UBA5 battery analyzer with constant current supplied at the rate $C/3$.

Table 1 Physical properties of the spinel compounds synthesized in this study

Organic reductant	a/Å	Z_{Mn}	Particle size^a/nm	Li/Mn ratio	Empirical formula	Theoretical capacity/mA h g^{-1}
Acetone	8.234	3.57	38	0.52	$Li_{1.02}Mn_{1.96}O_4$	127
Ethanol	8.220	3.64	22	0.55	$Li_{1.04}Mn_{1.91}O_4$	103
Hex-1-ene	8.212	3.62	14	0.52	$Li_{1.01}Mn_{1.93}O_4$	111
Isobutyraldehyde	8.226	3.54	18	0.51	$Li_{1.00}Mn_{1.98}O_4$	135
Propan-1-ol	8.226	3.61	27	0.51	$Li_{0.99}Mn_{1.94}O_4$	114
Propan-2-ol	8.223	3.53	28	0.51	$Li_{1.00}Mn_{1.98}O_4$	135

^{a} Determined from the Scherrer equation.

Results

Synthesis, structure, and morphology

In all of the hydrothermal reactions studied, spinel is the only solid product formed, except for reaction of $KMnO_4$ with methanol. Elemental analysis of the products indicates that our spinel compounds deviate slightly from the exact $LiMn_2O_4$ stoichiometry, with all products containing less Mn and having a Li/Mn ratio greater than 0.5. This gives formulas better represented as $Li[Li_xMn_{2-x}]O_4$, where some Li likely substitutes for Mn on the 16d Wyckoff sites. This formulation is supported by a smaller unit cell parameter determined by X-ray diffraction studies (a = 8.248 Å in $LiMn_2O_4$, JCPDS 35-782). Substitution of Li for Mn is known to occur in spinels synthesized at low temperatures.[25] In these compounds, the average Mn valence is greater than +3.5, which causes a unit cell contraction due to the smaller ionic radius of Mn^{4+} relative to Mn^{3+}. This is further evidenced by redox titration against Fe^{2+}. The unit cell parameters and primary crystallite sizes determined from XRD, the Mn oxidation states determined from redox titration, and Li : Mn ratios determined from ICP-AES, presented in Table 1.

Dwell times as short as 3 h give only spinel products in reactions using isobutyraldehyde, but 5 h was determined to be the shortest time required for obtaining the pure spinel phase at 180 °C, irrespective of the reductant employed. Longer heating periods did not have a noticeable effect on either the unit cell parameter or average crystallite domain size. Fig. 2 shows powder X-ray diffraction data of the solid state phases present at different stages of the reaction as well the experimental and calculated patterns for the spinel prepared *via* the oxidation of acetone. MnO_2 begins to precipitate at room temperature before the vessels are heated. The pXRD pattern for Li–birnessite was collected upon cooling the reaction after a 1 h dwell time. All of the organic reducing agents studied result in the same cubic spinel pattern as the sole phase after five hours, with the exception of methanol. Apparent ordered crystalline domain sizes (determined by the Scherrer equation, $\tau = k\lambda/\beta \cos\theta$) range from 10–30 nm, depending on the organic reductant employed. The primary particle size (τ) was determined from the FWHM (β) of a Lorentzian fit to the XRD peaks, which are quite broad. In addition to small particle size, the Scherrer equation also assumes a spherical particle shape (k = 0.9), but we note that microstrain in poorly crystalline structures can also attribute to line broadening, making it difficult to spot a particular trend in particle size from these data with respect to the organic reducing agent used.[26]

In order to determine the particle size, crystal habit, and morphology, we therefore turned to SEM imaging. Fig. 3 shows SEM images of compounds formed using each of the reductants used in this study. Of particular note, the nature of the organic reductant does not strongly influence particle morphology, as all of our samples exhibit large micron-sized aggregates of cubic, octahedral, and trigonal prismatic crystals. Typical crystals range in size from 15–40 nm, in agreement with our XRD data. However, a few large, very well defined crystals 100–300 nm in size are clearly interspersed. Interestingly, these larger crystals are much more populous in the samples prepared from iso-butyraldehyde and acetone than in those using the other
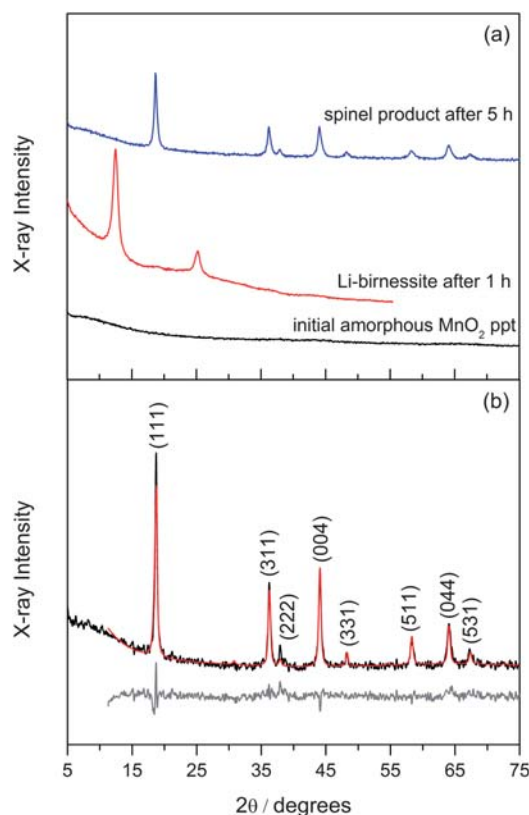

Fig. 2 X-Ray diffraction patterns of the inorganic products formed *via* permanganate oxidation of acetone. (a) Monitoring the products over the course of 5 h; (b) experimental (black), Rietveld refinement (red), and difference patterns (gray) of the spinel product with Miller indices indicated.
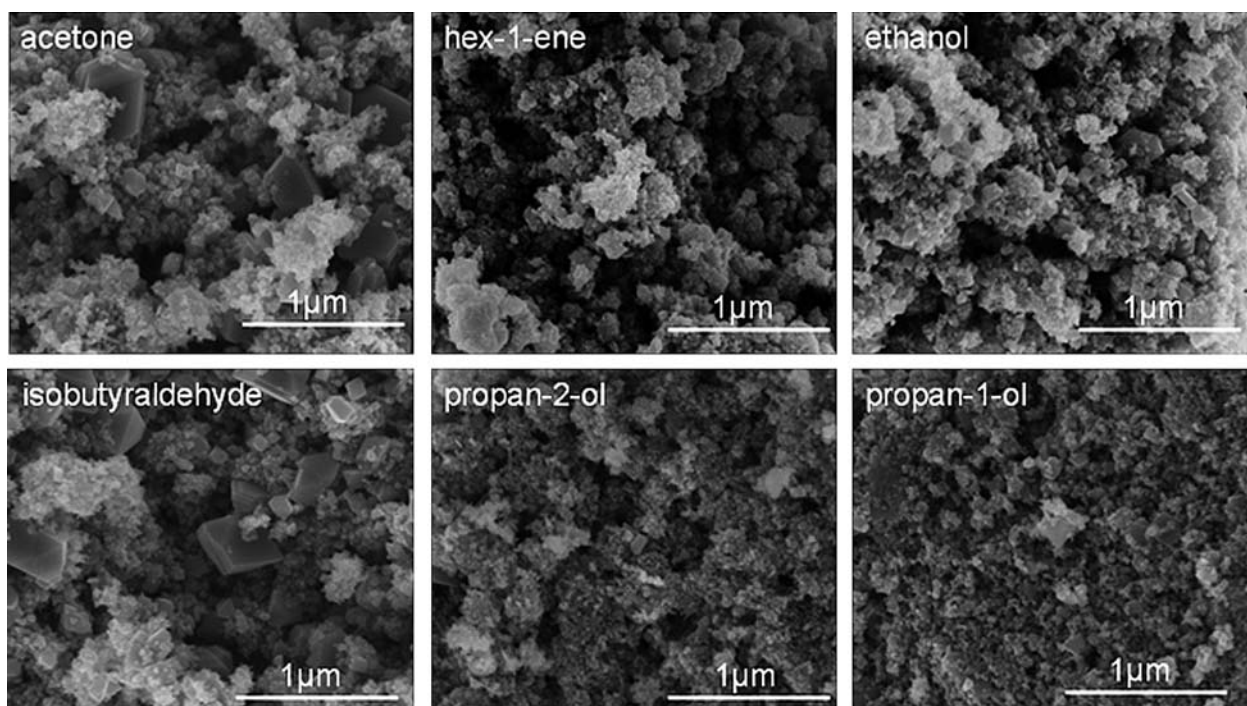
Fig. 3 SEM images of $Li_{1+x}Mn_{2-y}O_4$ spinel phases prepared *via* oxidation of the organic substrates listed.

organics. This prompted a mechanistic study into the organic transformation. For our studies of mechanism and electrochemistry in the following section, we focus our attention on the reaction of potassium permanganate with acetone, but note that the ESI† contains parallel results for each of the organic substrates employed.

Mechanism of spinel formation

Using organic reducing agents allows us to follow the reaction spectroscopically. As mentioned in the previous section, MnO_2 precipitates at room temperature at the concentrations used in our hydrothermal synthesis conditions. We can monitor the organic oxidation reaction by electronic absorption spectroscopy. The LMCT band of MnO_4^- in 0.1 M $LiOH_{(aq)}$ occurs at $\lambda_{max} = 525$ nm with a molar extinction coefficient, $\varepsilon = 2300$ M^{-1} cm^{-1}. Fig. 4a shows the time-resolved spectra for the oxidation of acetone. We note that in this kinetics study here, we have diluted our reactions by a factor of ten. The concentrations at which we carry out our hydrothermal reactions (~ 0.08 M MnO_4^-) cannot be studied directly in our UV-Vis spectrophotometer, as this is well outside of the Beer–Lambert Law range. As the organic oxidation occurs, MnO_4^- is converted to its one electron reduced product, MnO_4^{2-}, which disproportionates to form $MnO_{2(s)}$ and $MnO_4^-{}_{(aq)}$. Manganate has an absorption maximum at 605 nm that overlaps with the permanganate band. However, the spectra show a clean isosbestic point at 574 nm, indicating that only two species are absorbing. Due to this spectral overlap with MnO_4^{2-}, the absorbance at 525 nm never goes to zero.

All of the organic reducing agents we have studied with the exception of methanol go on to form spinel under hydrothermal reaction conditions. However, we note that initial disappearance of permanganate occurs at vastly different rates. Monitoring the
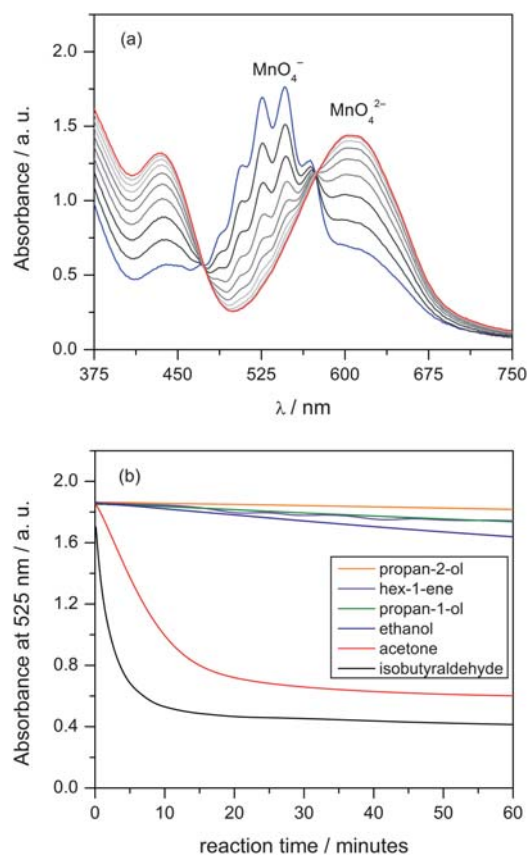

Fig. 4 UV-Vis spectra of the permanganate reduction. (a) One-electron reduction of MnO_4^- to MnO_4^{2-} using acetone; (b) monitoring the absorption at λ_{max} of 525 nm for all reductants that form spinel hydrothermally.

absorbance at 525 nm in Fig. 4b, we see that acetone and iso-butyraldehyde react with MnO_4^- most rapidly, while the alcohols and hex-1-ene react much more slowly. However, the linear dropoff in initial rate ceases after ∼7.5 minutes. This is in contrast to the typical reaction conditions used in our hydrothermal syntheses, where the starting solution, if left on the benchtop for 1 h becomes pale yellow with no remaining evidence of a water soluble manganese species (Fig. S7†).

We also studied the temperature-dependence of the reaction in order to learn more about the mechanism of the inorganic spinel formation. At lower temperature (160 °C), longer dwell times were required to afford pure product. Also, reactions conducted in the absence of any organic reducing agent result in no solid-state product formation after heating under our standard reaction condition of 5 h at 180 °C. With no organic reductant, reactions only give crystalline products when the temperature is increased above 200 °C and it is the monoclinic phase, Li_2MnO_3 that appears after 8 h, not spinel. Even after a 36 h dwell time, Li_2MnO_3 remains the only solid state product. It is surprising that Li–birnessite converts to Li_2MnO_3 under these conditions (as opposed to the spinel) considering the work done by Yanagisawa *et al.*, in which an independently prepared Li–birnessite sample is hydrothermally transformed to the spinel phase in 0.1 M LiOH at 150 °C.[18] The formation of Li_2MnO_3 in our case may be due to the higher temperature employed in our reaction, which is paradoxically required to first form Li–birnessite in the absence of an organic reductant.

Electrochemistry

A representative cyclic voltammogram of the spinel product resulting from oxidation of acetone, is illustrated in Fig. 5. At a scan rate of 0.1 mV s⁻¹, three redox waves are observed—one having $E_{1/2}$ of 2.9 and two closely spaced waves between 4.05 and 4.15 V, as has been well documented in the literature.[27] The electrochemical extraction of lithium from the occupied tetrahedral holes (8a sites) of $LiMn_2O_4$ occurs with concomitant oxidation of Mn at 4 V. Here, the average oxidation state of Mn increases from +3.5 to +4 upon charging. It has been shown that this process occurs in two steps observed by a 0.1 V separation in the redox waves. After one-half of the lithium has been removed,
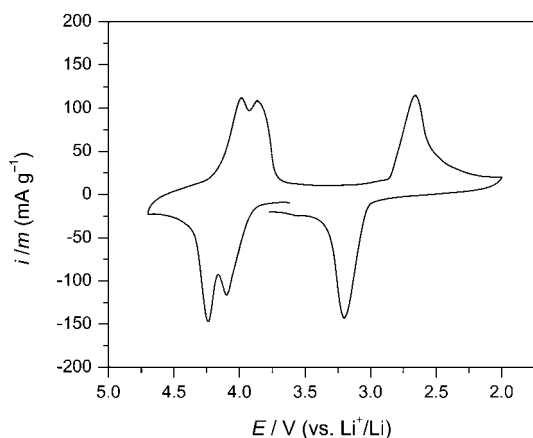
ordering of the remaining lithium atoms on the tetrahedral sites occurs. In this way, the cubic structure is retained as the unit cell contracts. Since the volume change is isotropic, this process is nondestructive, leading to electrochemically reversible waves in the cyclic voltammogram during Li⁺ extraction.

The redox wave at 2.9 V is due to the addition of Li to previously vacant octahedral holes (16c Wyckoff sites) to give $Li_2Mn_2O_4$ in the most reducing case.[18] In this electrochemical reaction, the average oxidation state of Mn decreases from +3.5 to +3. In contrast to 4 V cycling, this lithium insertion reaction has low reversibility, resulting in high capacity fade. This is attributed to a phase change from a cubic to a tetragonal unit cell, understood on the atomistic scale by Jahn–Teller distortion that occurs when the average manganese oxidation state falls below +3.5. In addition, Mn^{3+} disproportionates at the surface, and Mn^{2+} readily dissolves in the electrolyte solution. The formation of the tetragonal unit cell is accompanied by an anisotropic volume change leading to fracture of surface sites. Moreover, this mechanism also contributes to cycling fade at 4 V because the discharge from Mn_2O_4 to $LiMn_2O_4$ lowers the Mn oxidation state to less than +3.5 when even slightly over-discharged.[28] One approach to reduce the capacity fade when cycling about 4.1 V is to synthesize spinels with a small excess of lithium. Although aliovalent substitution of Li for Mn reduces the theoretical capacity of the material, it prevents the onset of Jahn–Teller distortion. It has been shown that a small amount of Li substitution in the system $Li_{1+x}Mn_{2-x}O_4$ ($x = 0.03–0.05$) is optimal to decrease capacity fade while minimizing the loss of available capacity.[29,30]

Galvanostatic cycling experiments shown in Fig. 6 were conducted at the charge/discharge rate of $C/3$ (constant current applied to charge the theoretical capacity of the battery in 3 hours) for the voltage range 4.4 to 3.5 V to give a capacity of 105 mA h g⁻¹ for the sample prepared from acetone oxidation, nearly identical to that observed for other reported nanoscale $LiMn_2O_4$ particles.[16] The first charge and discharge cycles are anomalous, which is commonly observed as the solid–electrolyte interface (SEI layer) forms. From the second cycle on, we observe two steps in the discharge curve—centered about 4.05 and 3.90 V with an inflection point at ∼3.97 V, indicative of the reversible cubic cell contraction/expansion over the course of cycling. Due to this reversibility, we observe no significant capacity fade (<2%) over the first 10 charge/discharge cycles, in excellent agreement with previous studies on lithium rich spinels.[5] As mentioned, the larger average Mn valence of +3.57 results in a diminished theoretical capacity (127 *cf.* 148 mA h g⁻¹ for stoichiometric $LiMn_2O_4$). However, we note that in typical batteries, approximately 6–10% of Li⁺ remains in the structure upon cycling about 4 V, and the full capacity is achieved only when the potential exceeds 4.5 V, which challenges the operating limits of the polycarbonate electrolyte solution.[31] After 100 cycles at this rate, we note that our sample prepared using acetone loses 13% of its discharge capacity, illustrated in Fig. 6. This loss is likely due to the instability of Mn^{3+} at the surface, compounded in our case by the use of $LiPF_6$ as the electrolyte which inevitably contains trace HF impurities known to promote this manganese dissolution process.[32]

The first ten discharge cycles for the other organic reducing agents employed are shown in Fig. 7a. The trend in observed

Fig. 5 Cyclic voltammogram of $Li_{1.02}Mn_{1.96}O_4$ synthesized from the oxidation of acetone.
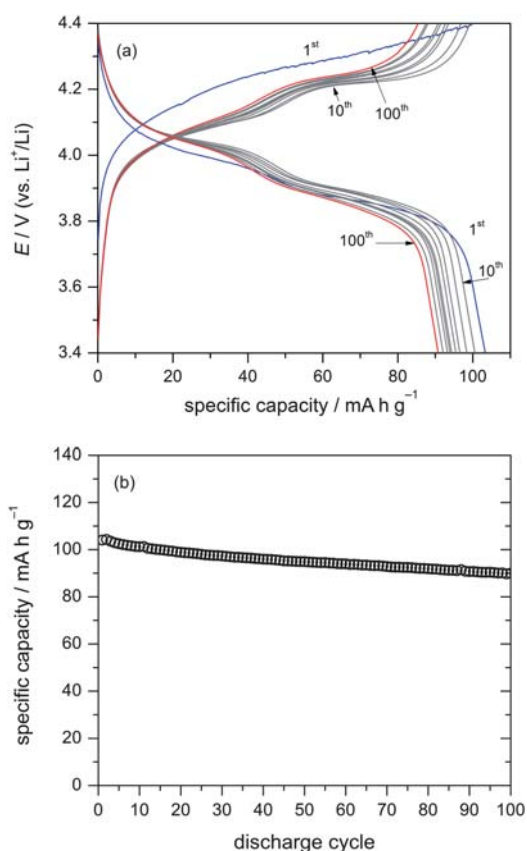
Fig. 6 Galvanostatic cycling of $Li_{1.02}Mn_{1.96}O_4$ synthesized from the oxidation of acetone.

Fig. 7 Galvanostatic cycling for spinels prepared *via* reduction of the organic reductants employed. (a) First ten discharge cycles; (b) relationship between specific capacity and rate of MnO_4^- reduction.

discharge capacities for the series correlates with the kinetics data obtained in the previous section. With faster one electron reduction of MnO_4^-, more 100–300 nm crystallites result in the hydrothermal spinel product. Fig. 7b shows the observed capacity as a function of absorbance after 1 hour. This time was chosen as our comparison point because we know from our hydrothermal reactions that the solid-state inorganic intermediate, Li–birnessite, forms within this timeframe. Again, we note that the concentration of MnO_4^- in our actual reactions is ten times higher, thus we plot absorbance rather than $[MnO_4^-]$. Interestingly, the theoretical values calculated from the composition data correlate with the observed capacities as well, with the notable exception of propan-2-ol whose observed initial discharge capacity (79 mA h g^{-1}) is significantly lower than that of the acetone sample despite having a higher theoretical charge capacity. This underscores the importance of morphology over composition in the narrow range of compositions our organic oxidation reactions afford. The spinel compounds with the highest overall capacities, namely acetone and isobutyraldehyde, react most rapidly, and both exhibit a greater number of larger 100–300 nm crystallites.

Discussion

This simple reaction takes advantage of one of the oldest known synthetic organic reactions—the use of $KMnO_4$ to oxidize unsaturated and functionalized organic molecules. While the vast

majority of research on these reactions has centered on the mechanism of organic product formation, far centered on the mechanism of organic product formation, far less attention has been given to the utility of the subsequent manganese oxide inorganic byproducts towards novel oxide synthesis. In the exploratory work presented here, spinel is the sole solid-state product of the reaction, regardless of organic reductant employed. Moreover, the morphology of the product is conserved, regardless of the rate of the organic oxidation, hinting that a common inorganic intermediate is formed. This is confirmed by the appearance of Li–birnessite in each reaction after short reaction times. In accord with what is known about permanganate oxidations in organic chemistry, soon after addition of the organic reductant, the purple color of permanganate gives way to the green color of the one-electron reduced manganate ion (MnO_4^{2-}). The manganate ion is unstable in moderately alkaline solutions, and it quickly disproportionates leading to the precipitation of brown, amorphous, MnO_2 and additional MnO_4^-.[33] We note that this disproportionation is interesting in that it results in the reformation of starting MnO_4^-. This proposed pathway and its corresponding Latimer diagram is shown in Scheme 1. In dilute basic solutions of acetone, permanganate is easily reduced to form the observed amorphous MnO_2 phase and acetone is oxidized to form pyruvaldehyde, as confirmed by NMR spectroscopy (Fig. S8†). The reaction occurs

$$MnO_4^- \xrightarrow[\text{red} \quad \text{ox}]{} MnO_4^{2-}$$

$$3MnO_4^{2-} + 2H_2O \rightleftharpoons MnO_2(s) + 2MnO_4^- + 4OH^-$$

$$MnO_4^- \xrightarrow{0.56\ V} MnO_4^{2-} \xrightarrow{0.27\ V} MnO_4^{3-} \xrightarrow{0.93\ V} MnO_2$$

$$\text{(0.60 V)}$$

Scheme 1

within minutes on the benchtop at room temperature. We note that the driving force for the 3-electron reduction of MnO_4^- to form amorphous MnO_2 can be estimated by the Nernst equation, $E = E^\circ - 0.059 \times (pH)$. The measured pH of our reaction both before and after the precipitation of MnO_2 on the bench is 12.5, giving an estimated reduction potential of 0.96 V. This estimate should suffice given the dilute nature of our reactions. The large driving force gives rise to rapid reduction of organic substrates, and combining our UV-Vis experiment with SEM imaging, we deduce that particle size relates directly to the rate of organic oxidation.

Under true synthesis concentrations ($\sim$0.08 M MnO_4^-), our observations hold up. Adding a basic solution of potassium permanganate to the aldehyde and acetone organic substrates employed results in a nearly instantaneous reaction, judged by the loss of color and precipitation of MnO_2. In contrast, hex-1-ene and the alcohols take several minutes before we observe the precipitation of the intractable brown solid MnO_2 at room temperature. Honing in on the alcohols, we note that oxidation of ethanol and both propanol isomers resulted in the desired spinel phase, while reaction with methanol gave brown powders of poor crystallinity, with weak diffraction peaks corresponding to the Li–birnessite phase, $LiMnO_2$ (Fig. S9†). Preparing $LiMnO_2$ is well documented in the chemistry of manganese oxides, and isolating the reaction product formed after short heating periods (1 hour) reveals this layered structure for all our syntheses. $LiMnO_2$ is a known intermediate in other reported hydrothermal methods that result in spinel.[18] This reaction is sluggish at temperatures less than 180 °C.

The balanced equation for the oxidation of acetone to form pyruvaldehyde is:

$$3Me_2CO + 4MnO_4^- \rightarrow$$
$$3Me(CO)CHO + H_2O + 4OH^- + 4MnO_2$$

However, we note that reactions carried out stoichiometrically do not ultimately yield spinel. Our hydrothermal reaction conditions involve a small excess of reductant with no evidence of remaining MnO_4^- observed when the reactions are complete. The ultimate fate of the remaining permanganate is unclear, although a reasonable possibility is that it reacts further by oxidizing the organic products generated from the initial step. This is substantiated by our observation that methanol is not a viable reductant for the formation of spinel phases. In this case, unreacted permanganate persists upon cooling our hydrothermal vessels, and the expected methanol oxidation products,

formaldehyde and formic acid, would be poor reductants for further reaction. In each of the other reductants studied, the reaction yields are nearly quantitative in manganese. We are further investigating the mechanism of this reaction by analyzing the organic products and mapping the inorganic species present over the course of the reaction. What we do know is that the amorphous MnO_2 that precipitates from the oxidation of acetone can be used to produce spinel, as determined by XRD (Fig. S10†). However, spinel prepared from heating the isolated room temperature precipitate shows extremely poor capacity (<20 mA h g^{-1}). The MnO_2 precipitate is shaped like 200–500 nm branches of cauliflower, illustrated in Fig. 8. Thus, we hypothesize that any MnO_2 present under hydrothermal conditions is either a different morphology than what we observe at room temperature or that MnO_2 simply does not precipitate at the higher temperatures and pressures afforded by hydrothermal synthesis. That is, our results suggest that reaction does not simply form electrolytic-grade-like MnO_2. The important consequence is that the manganese intermediates generated under our hydrothermal conditions are sufficiently reactive to yield pure spinel products after a short 5 h dwell time.

The alcohols react most slowly at room temperature under higher concentrations, which is expected as their proposed mechanisms involve initial, pre-oxidation, rate-limiting steps. Curiously, Greer and Wiberg originally proposed the slow formation of an enolate ion as the initial, rate-limiting step in the oxidation of acetone based on the first order dependence on hydroxide ion concentration, while reactions with alcohol to give aldehydes in alkali solutions proceed through either a hydride or hydrogen-atom transfer between the alkoxide and permanganate prior to oxidation as the rate determining step.[34–36] Aldehydes and olefins do not have such pre-oxidation steps and react with permanganate at a much faster rate.[37,38] In the spectroscopic study presented here, we have only examined the reduction of MnO_4^-, not the rate of organic product formation.

For the inorganic reaction, we cannot rule out the possibility that potassium cations from our $KMnO_4$ reactant may be capable of intercalating into birnessite structure, but are unable to template spinel formation due to their large size. Rather, K$^+$ intercalation into birnessite templates the formation of hollandite, the α-MnO_2 structure having larger 2×2 tunnels.[18] In our case,

Fig. 8 Amorphous MnO_2 precipitate resulting from the room-temperature oxidation of acetone.

however, this phase was not observed in any XRD patterns, and we found no potassium incorporation into any of the solids as determined by our ICP measurements. The least understood aspect of these reactions is the sequence by which amorphous MnO_2 transforms to crystalline Li–birnessite. Although this transformation has been recognized in work by Wang et al., in which $(CTA)MnO_4$ was used to synthesize $LiMn_2O_4$ hydrothermally,[24] no specific mechanism is proposed. We are currently investigating the mechanism of this transformation, including probing further all of the oxidized organic products, and these mechanistic aspects will be addressed in a future report from our group.

Conclusions

We have demonstrated a simple, one-pot, hydrothermal synthesis of nanocrystalline lithium manganese oxide spinel using only LiOH, $KMnO_4$ and an inexpensive organic reductant. This reaction eliminates the need for a separate permanganate reduction step or cation-exchange to form a suitable manganese precursor. To the best of our knowledge, $KMnO_4$ has never been used directly in the hydrothermal synthesis of lithium manganese oxide spinels, making this preparation attractive due to the low cost and high availability of precursors. These factors weigh heavily on the viability of materials for use in large-scale energy storage applications. Although the spinel structure of $Li_{1+x}Mn_{2-y}O_4$ forms regardless of the choice of organic reductant, different organic reducing agents show different crystallite sizes by SEM, and the particle size relates to the initial rate of permanganate reduction. This affords us a facile method of predicting and controlling particle size. Our spinel $Li_{1+x}Mn_{2-y}O_4$ products have small substitution of Li for Mn, necessary for good electrochemical performance, with capacity fade upon cycling that is less than that observed for stoichiometric $LiMn_2O_4$.

Acknowledgements

Notes and references

1 J. W. Fergus, J. Power Sources, 2010, 195, 939.
2 Handbook of Battery Materials, ed. J. O. Besenhard, Wiley-VCH, New York, 1998.
3 M. Armand and J. M. Tarascon, Nature, 2008, 451, 652.
4 M. M. Thackeray, J. Am. Ceram. Soc., 2004, 82, 3347.
5 D. Guyomard and J. M. Tarascon, Solid State Ionics, 1994, 69, 222.
6 M. M. Thackeray, P. J. Johnson, J. T. Vaughey, N. Li and S. A. Hackney, J. Mater. Chem., 2005, 15, 2257.
7 C. H. Jiang, S. X. Dou, H. K. Liu, M. Ichihara and H. S. Zhou, J. Power Sources, 2007, 172, 410.
8 M. M. Thackeray, W. I. F. David, P. G. Bruce and J. B. Goodenough, Mater. Res. Bull., 1983, 18, 461.
9 A. Momchilov, V. Manev and A. Nassalevska, J. Power Sources, 1993, 41, 305.
10 K. Mizushima, P. C. Jones, P. J. Wiseman and J. B. Goodenough, Mater. Res. Bull., 1980, 15, 783.
11 M. Broussely, P. Biensan and B. Simon, Electrochim. Acta, 1999, 45, 3.
12 D. G. Wickham and W. J. Croft, J. Phys. Chem. Solids, 1958, 7, 351.
13 P. Barboux, J. M. Taracson and F. K. Shokoohi, J. Solid State Chem., 1991, 94, 185.
14 D. Im and A. Manthiram, J. Electrochem. Soc., 2002, 149, A1001.
15 X. Li, R. Xiang, T. Su and Y. Qian, Mater. Lett., 2007, 61, 3597.
16 M. Okubo, Y. Mizuno, H. Yamada, J. Kim, E. Hosono, H. Zhou, T. Kudo and I. Honma, ACS Nano, 2010, 4, 741.
17 S. W. Donne, A. F. Hollenkamp and B. C. Jones, J. Power Sources, 2010, 195, 367.
18 Q. Feng, K. Yanagisawa and N. Yamasaki, J. Porous Mater., 1998, 5, 153.
19 M. S. Whittingham and P. Y. Zavalij, Solid State Ionics, 2000, 131, 109.
20 A. Manthiram, J. Kim and S. Choi, Mater. Res. Soc. Symp. Proc., 2000, 575, 9.
21 Z. Liu, W. Wang, X. Liu, M. Wu, X. Wu, M. Li and Z. Zeng, J. Solid State Chem., 2004, 177, 1585.
22 H. Yue, X. Huang, D. Lv and Y. Yang, Electrochim. Acta, 2009, 54, 5363.
23 A. A. Zinov'ev and K. V. Titova, Zh. Neorg. Khim., 1963, 8, 1579.
24 W. Wang, H. Jiang, Z. Liu and X. Liu, J. Mater. Chem., 2005, 15, 1002.
25 H. Kaiya, S. Suzuki and M. Miyayama, Key Eng. Mater., 2009, 388, 41.
26 V. K. Pecharsky and P. Y. Zavalij, Fundamentals of Powder Diffraction and Structural Characterization of Materials, Kluwer Academic Publishers, Boston, MA, 2003.
27 E. V. Makhonina, V. S. Pervov and V. S. Dubasova, Russ. Chem. Rev., 2004, 73, 991.
28 G. G. Amatucci, C. N. Schmutz, A. Blyr, C. Sigala, A. S. Gozdz, D. Larcher and J. M. Tarascon, J. Power Sources, 1997, 69, 11.
29 R. J. Gummow, A. de Kock and M. M. Thackeray, Solid State Ionics, 1994, 69, 59.
30 G. G. Amatuci, N. Pereira, T. Zheng, I. Plitz and J. M. Tarascon, J. Power Sources, 1999, 81, 39.
31 J. B. Goodenough and Y. Kim, Chem. Mater., 2010, 22, 587.
32 A. du Pasquier, A. Blyr, A. Cressent, C. Lenain, G. Amtucci and J. M. Tarascon, J. Power Sources, 1999, 81, 54.
33 A. Manthiram, J. Kim and S. Choi, Mater. Res. Soc. Symp. Proc., 2000, 575, 9.
34 K. B. Wiberg and R. D. Greer, J. Am. Chem. Soc., 1965, 87, 5202.
35 D. G. Lee and T. Chen, J. Org. Chem., 1991, 56, 5341.
36 Oxidation in Organic Chemistry, ed. K. B. Wiberg, Academic Press Inc, London, 1965.
37 S. Dash, S. Patel and B. K. Mishra, Tetrahedron, 2009, 65, 707.
38 M. Jàky and J. Szammer, J. Phys. Org. Chem., 1997, 10, 420.